Title: Fe-S centers of proteins as a molecular target of toxicity for a complex transition metal oxide nanomaterial

Nicholas J Niemuth[1], Yonqian Zhang[2], Aurash A Mohaimani[1], Angela Schmoldt[1], Elizabeth D Laudadio[2], Robert J Hamers[2], Rebecca D Klaper[1]*

[1] School of Freshwater Sciences, University of Wisconsin-Milwaukee, 600 E Greenfield Ave., Milwaukee, WI 53204

[2] Department of Chemistry, University of Wisconsin-Madison, 1101 University Ave., Madison, WI 53706

* Corresponding author: rklaper@uwm.edu

Abstract

Previous studies of biological impacts of transition metal oxide (TMO) nanomaterials have demonstrated oxidative stress as a mechanism of toxicity. However, these studies rarely identify the specific underlying molecular targets responsible for phenotypic impacts in organisms. Our previous study demonstrated significant negative impacts of lithium cobalt oxide (LCO) nanomaterials on growth, development, hemoglobin, and gene expression for heme synthesis in larvae of model sediment invertebrate *Chironomus riparius*. In this study, we propose that the alteration of Fe-S protein function by LCO is a molecular initiating event that leads to these changes. Using electron paramagnetic resonance (EPR) spectrometry of intact larvae we show oxidation of the aconitase 4Fe-4S center after LCO exposure, and a reduction in aconitase activity. Next-generation RNA sequencing identified significant changes in expression of genes involved in 4Fe-4S center binding, Fe-S center synthesis, iron ion binding, and metabolism. Specifically, expression of citrate cycle and electron transport chain Fe-S protein genes *succinate*

dehydrogenase and *NADH dehydrogenase* are upregulated, and EPR indicates that their complex I and II Fe-S centers are increased. Our results point to oxidation of metabolic and regulatory Fe-S centers of proteins as a potential molecular mechanism underlying observed impacts of LCO on growth and development by impacting metabolic homeostasis, a mechanism which may apply for these conserved proteins across species and for other TMO nanomaterials.

Keywords: adverse outcome pathway, molecular initiating event, nanotoxicity, iron-sulfur protein, electron paramagnetic resonance, transition metal oxides

TOC Art

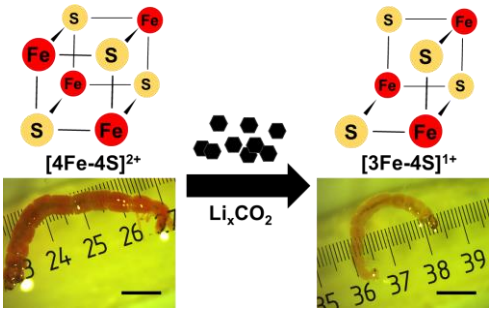

33 In the past two decades substantial work has occurred toward understanding potential
34 implications of increasing commercial use of engineered nanomaterials (ENMs) on human health
35 and the environment. Over this period, studies of ENM impacts grew from basic toxicity
36 exposures to increasingly sophisticated studies aimed at understanding how ENM properties
37 determine toxicity, mechanisms by which materials interact with biological systems, and how
38 and what materials and their environmental transformations may be of potential concern.[1,2] To
39 date nanotoxicology has focused largely on first-generation ENMs (*e.g.* Au, Ag).[3] When an
40 underlying mechanism is proposed, toxicity is frequently attributed to reactive oxygen species
41 (ROS).[4–7] ROS have long been classified as damaging.[8] However, research within the last decade
42 has revealed ROS as important signaling molecules generated by cells[9,10] involved in regulating
43 fundamental biological processes including metabolism,[11] proliferation,[12] development,[13]
44 autophagy[14] and apoptosis.[15] Thus, ROS as a universal explanation for nanotoxicity is not
45 explanatory or mechanistic, and its blanket assertion may be limiting advancement of our
46 understanding of nano-bio interactions.

47 Recently, increasing effort has been made to identify the initial molecular interaction between
48 nanoparticles and cellular components of organisms, or molecular initiating event, that triggers
49 the key events that lead ultimately to a phenotypically observable adverse outcome, *e.g.*
50 decreased reproduction or survival. Despite these efforts, identification of specific molecular
51 initiating events for nanomaterial exposures is still rare in the literature, and studies are usually
52 limited to identifying key events and adverse outcomes.[16–18] Finding specific, testable molecular
53 initiating events is necessary for identify unifying mechanisms of nanotoxicity applicable across
54 nanomaterials and organisms. Within this Adverse Outcome Pathway (AOP) framework,
55 observed ROS, if acting as signaling molecules, may be correlative rather than causative and a

key event in the AOP rather than the molecular initiating event.[19] Singling out ROS as the molecular initiating event in a nanotoxicity AOP requires identifying specific molecular targets of ROS that lead to key events and ultimately to adverse outcomes in exposed organisms.

Complex transition metal oxides (TMOs) are a category of next-generation ENM where two or more transition metals are incorporated with oxygen into a crystalline lattice. Lithium cobalt oxide (LCO) and related compositions are complex TMOs with large and growing commercial use as the active cathode material of lithium ion batteries (LIBs) in consumer electronics and electric vehicles.[20–23] Due to large manufacturing volume and a dearth of recycling facilities, LIB waste is expected to accumulate in landfills, and accidental release of LCO and related compounds from landfill leachate or manufacturing presents a potential environmental concern.[24,25] In 2016, 374 kilotons of LIBs were in use, and LIB waste from electric vehicles alone is expected to reach 200 kilotons annually by 2025.[24] LIB waste was shown to leach 164 g Co per kg of battery, 16% of its total mass.[24]

LCO can aggregate and settle in aquatic systems, creating particularly high exposure concentrations for sediment-dwelling organisms. *Chironmus riparius* is a model sediment-dwelling invertebrate used for sediment toxicity assays, including for ENMs, and is important in many freshwater systems, with larval stages that reside in the sediment where they consume detritus from silt particles, eventually emerging as adult flies.[26–32] We showed previously that exposure to 10 mg/L LCO for 7 d significantly reduced growth and increased time to adult emergence for *C. riparius* larvae, as well as reducing larval hemoglobin and levels of heme synthesis gene *porphobilinogen synthase*.[33]

These results suggested a key event for LCO toxicity in which exposure disrupts normal heme synthesis in exposed larvae. Synthesis of heme and iron metabolism more broadly is regulated by

79 the iron-responsive protein (IRP1), whose mRNA-binding activity is governed by the status of its
80 Fe-S center. This $[4Fe\text{-}4S]^{2+}$ center also allows IRP1 to act as an aconitase (ACO1), converting
81 citrate to isocitrate in the citric acid cycle.[34–37] Both heme synthesis and energy metabolism are
82 thus dependent on this Fe-S center's status, which has been shown to be sensitive to ROS.[38]
83 Many other important metabolic enzymes including succinate dehydrogenase and NADH
84 dehydrogenase (involved in the citrate cycle and the electron transport chain) require Fe-S
85 centers for their activity.[35,39–42] Thus, the growth and development defect adverse outcomes
86 observed in LCO-exposed larvae, along with the key event of dysregulation of hemoglobin and
87 heme synthesis,[33] suggest that *C. riparius* LCO toxicity could occur by the molecular initiating
88 event of Fe-S center disruption in regulatory and enzymatic proteins. These proteins are
89 ubiquitous across bacterial, animal, and plant kingdoms; indicating impacts on Fe-S centers
90 could be a molecular initiating event common to TMO nanomaterials across species, potentially
91 providing a framework for understanding the impacts of these materials more broadly.[42]

92 This molecular mechanism of LCO toxicity has not previously been explored, with previous
93 studies attributing LCO impacts to generic ROS.[43–45] Prior studies of LCO's biological impacts
94 showed production of ROS in trout epithelial cells,[45] with possible direct production of ROS due
95 to its Co^{3+} oxidation state.[46] Here we test the hypothesis that the disruption of Fe-S centers could
96 be the molecular initiating event causing observed adverse outcomes. Oxidation by ROS
97 transforms the aconitase $[4Fe\text{-}4S]^{2+}$ site into an enzymatically inactive $[3Fe\text{-}4S]^{1+}$ visible by
98 electron paramagnetic resonance (EPR).[38] We used EPR to examine the oxidation state of the Fe-
99 S protein aconitase and examined its enzyme activity to determine the impact of LCO on this
100 protein as one of the important Fe-S proteins that may be impacted by exposure in larvae. We
101 also used next-generation RNA sequencing to gain an overall picture of the impacts of LCO

exposure on molecular pathways in *C. riparius*. Together, these techniques demonstrate oxidation of the aconitase Fe-S center and inhibition of its activity in LCO-exposed larvae accompanied by broad metabolic disruption, including of critical Fe-S protein genes and their associated metabolic pathways. These results support an AOP whereby oxidative disruption of Fe-S centers by LCO perturbs normal metabolism, negatively affecting growth and development of *C. riparius*. The abundance of these proteins across the evolutionary tree highlights the importance of this interaction as a potential unifying mechanism for nano-bio interactions of TMO nanomaterials.

Results and Discussion

LCO causes aconitase Fe-S center oxidation, reduces aconitase enzyme activity, and changes the abundance of Fe-S centers of other proteins

Impacts of LCO on the Fe-S centers of *C. riparius* larvae were evident from whole-animal EPR spectra (Fig 1). Significant increases were observed in the level of oxidized aconitase $[3Fe\text{-}4S]^{1+}$ in animals exposed to 10 mg/L LCO for 7 d (Fig 1b; One-way Welch ANOVA, Dunnett T3 post-hoc $p < 0.05$). Oxidation of the aconitase $[4Fe\text{-}4S]^{2+}$ center to the inactive but EPR-visible $[3Fe\text{-}4S]^{1+}$ would be expected to negatively affect metabolism,[38,41] and metabolic defects could underlie the reduced size and delayed development observed to result from 10 mg/L LCO exposure in our previous study.[33] Cobalt alone has also been shown to impact function of Fe-S centers in bacteria and impact oxidative metabolism,[41,47] however, this is the first study to our knowledge showing impacts on Fe-S centers by EPR in a whole multicellular organism as well as the first exploration of this mechanism of toxicity for an ENM.

124 Impacts of LCO on the Fe-S center of aconitase was confirmed by aconitase activity assays on
125 extracted larval protein. Aconitase activity of protein extracted from *C. riparius* larvae exposed
126 to LCO at 10 mg/L for 48 hr was significantly reduced compared to control and ion treatment
127 (Fig 2; One-way ANOVA, Tukey HSD post-hoc $p < 0.05$). While transcripts for both cytosolic
128 and mitochondrial aconitase were identified by RNA-Seq, expression did not differ significantly
129 between LCO exposures and controls. Lack of expression change at the transcript level along
130 with observation of increased oxidation of the aconitase Fe-S center by EPR (Fig 1b) suggest
131 that observed reduction in activity is likely due to oxidation of the solvent-exposed aconitase
132 $[4Fe\text{-}4S]^{2+}$ to the inactive $[3Fe\text{-}4S]^{1+}$ as a result of LCO exposure. Reduced aconitase activity as
133 a result of LCO exposure would be expected to cause disruptions to metabolism that could
134 underly reduced larval size and delayed development observed in our previous study.[33]

135 We also observed significant increases in the $[2Fe\text{-}2S]^{1+}$ and $[4Fe\text{-}4S]^{1+}$ centers of complex I and
136 II NADH dehydrogenase and succinate dehydrogenase from EPR spectra (Fig 1c; One-way
137 Welch ANOVA, Dunnett T3 post-hoc $p < 0.05$). The $[3Fe\text{-}4S]^{1+}$ center of succinate
138 dehydrogenase also showed an increasing trend for ion and LCO-exposed animals but was not
139 significantly different from control (Fig 1d; One-way Welch ANOVA, Dunnett T3 post-hoc $p >$
140 0.05). NADH dehydrogenase comprises part of electron transport chain (ETC) complex I.
141 Succinate dehydrogenase functions as part of the citric acid cycle and as part of complex II of the
142 ETC. The Fe-S centers of these proteins are embedded within a protein complex where they
143 shuttle electrons.[39,40] The Fe-S centers of complex II have been shown to be relatively insensitive
144 to oxidation by ROS as compared with aconitase,[48] which may be due to their being buried in
145 protein while the aconitase 4Fe-4S is solvent exposed. An increase in the levels of complex I and
146 II Fe-S centers suggests potential compensation for LCO impacts: increased Fe-S synthesis to

147 compensate for Fe-S oxidation, increased ETC activity to compensate for metabolic
148 impairments, or both.

149

150 ***Global gene expression changes support importance of LCO impacts on Fe-S centers and***
151 ***metabolism***

152 The impacts of LCO on Fe-S centers were also evidenced by gene expression changes observed
153 by RNA-Seq. Thirteen genes with molecular functions associated with Fe-S proteins directly and
154 many others associated with downstream functions related to Fe-S genes were differentially
155 expressed. Table 1 shows differentially expressed genes (Wald FDR < 0.1) with molecular
156 functions related to Fe-S binding between control and 10 mg/L LCO-exposed larvae.[49,50] These
157 include genes involved in assembly of 4Fe-4S centers: *NUBP1*, *NUPB2*, and *ISCA2*. *ISCS*,
158 involved in assembly of 2Fe-2S centers, is also significantly upregulated.[51] In addition, genes for
159 important Fe-S center-containing enzymes succinate dehydrogenase and NADH dehydrogenase,
160 involved in the citrate cycle and oxidative phosphorylation, were also significantly
161 upregulated.[39,40] The Fe-S centers of succinate dehydrogenase and NADH dehydrogenase were
162 also observed to be increased in 10 mg/L LCO-exposed larvae versus controls by EPR (Fig 1c).
163 Upregulation of Fe-S center-containing DNA repair protein genes *endonuclease III* and *RTEL1*
164 suggest that LCO-exposed larvae could be more sensitive to DNA damage due to impacts on
165 repair proteins that require Fe-S centers for their function.

166 Genes related to iron and iron ion binding and 4Fe-4S binding were significantly enriched among
167 genes differentially expressed between control and 10 mg/L LCO exposures (Figure 3;
168 Benjamini-adjusted FDR < 0.1). This also supports the hypothesis that iron metabolism is

169 disrupted by LCO exposure (observed in Niemuth *et al*. 2019 as reduced hemoglobin in LCO-
170 exposed larvae)[33] and the specific hypothesis that impacts of LCO on Fe-S centers could underlie
171 observed impacts on iron metabolism and metabolism more generally.

172 Our previous research suggested that broader metabolism may be impacted by LCO exposure,[33]
173 which is supported here, as metabolic pathways are significantly enriched with 156 genes
174 differentially regulated (Fig 3; Benjamini-adjusted FDR < 0.001). Of the 319 KEGG orthologies
175 that map to pathways, 156, or nearly half, are involved in metabolic pathways. The distribution
176 of up and downregulation of genes in these pathways suggest an upregulation of genes involved
177 in energy production (Fig 4) and downregulation of processes that use energy (Fig 4, Supp Fig
178 S1). For example, genes involved in glycolysis/gluconeogenesis (14 genes), the citrate cycle (7
179 genes), and oxidative phosphorylation (17 genes) are all upregulated (Fig 4). Decreased protein
180 processing (Supp Fig S1), changes in amino acid metabolism toward catabolism, and
181 downregulation of lipid metabolism all suggest increases in energy production with concomitant
182 decreases in energy use and storage (Fig 4). In addition, changes in genes involved in PI3K-Akt
183 and AMPK signaling suggest regulatory changes toward energy production and away from
184 energy use in cells and tissues (Supp Fig S2). Changes in autophagy (8 genes; Supp Fig S3),
185 glucagon signaling (11 genes), insulin signaling (6 genes), and retrograde endocannobinoid
186 signaling (14 genes) also indicate changes toward energy production and uptake (Supp Fig S4).
187 This result, along with significant enrichment for specific metabolic pathways including carbon
188 metabolism, lipid metabolism, glycolysis/gluconeogenesis, and amino acid metabolism (Fig 3;
189 Benjamini-adjusted FDR < 0.1) support the hypothesis proposed in Niemuth *et al*. 2019 that
190 changes observed in size and development of LCO-exposed larvae may be the results of
191 metabolic effects.

192 Given the conservation across species of Fe-S proteins involved in processes such as heme
193 synthesis (*e.g.* ferredoxin, ferrochelatase), iron homeostasis (*e.g.* IRP1), energy metabolism (*e.g.*
194 aconitase, NADH dehydrogenase, succinate dehydrogenase), and DNA repair (*e.g.* endonuclease
195 III),[42] changes in these centers due to LCO exposure would be expected to have broad impacts
196 on cellular processes, both in *C. riparius* and in other species. Observations of increased iron
197 associated with LCO exposure in mouse lung[44] and decreased expression of heme-containing
198 *catalase* in *Daphnia magna*[43] suggest this mechanism may indeed apply to other organisms. This
199 mechanism may also be indicated for other transition metal oxide nanomaterials. Specifically,
200 components of pathways found to be significantly impacted in our results (Figs 2, 3, and 4) have
201 been shown to be affected by exposure to TMO nanomaterials in other studies, including:
202 decreased aconitase activity in liver of ZnO-exposed white sucker;[57] changes in expression of
203 aconitase, succinate dehydrogenase, and other citrate cycle genes in *Pseudomanas aeruginosa*
204 exposed to CuO ENMs;[58] increased expression of electron transport chain proteins from
205 exposure to ZnO, TiO_2, and CuO nanoparticles in mouse hepatocytes;[59] increased
206 gluconeogenesis from ZnO particles in rat liver cells;[52] decreases in succinate and citrate
207 (involved in the citrate cycle) and hemoglobin in ZnO-exposed rat kidney;[53] negative impacts of
208 TiO_2 on carbon metabolism in algae;[55] and decreases in citrate cycle metabolites from TiO_2
209 exposure in *C. elegans*.[56] Although impacts of materials specifically on Fe-S centers were not
210 explored in these studies, the impacts observed in this study and the relevance of Fe-S proteins to
211 the observed impacts may recommend broader investigation of this mechanism in future TMO
212 nanomaterial toxicity studies.

213

214

215 ***Additional molecular impacts identified by RNA-Seq***

216 One molecular function significantly enriched among differentially expressed genes between
217 control and LCO 10 mg/L exposures (Benjamini-adjusted FDR < 0.001) not related to Fe-S
218 proteins was chitin binding and metabolism (49 genes, Fig 3). Chitin is a biopolymer important
219 in the formation of invertebrate exoskeletons as well as the protective peritrophic matrix of the
220 gut.[60] Included among the differentially expressed genes with functions related to chitin binding
221 and metabolism are a number of peritrophins (*e.g. Peritrophin 1*, *Peritrophin 44*, *Obstractor b*),
222 involved in reorganizing the peritrophic matrix that protects the gut. Reorganization of the
223 peritrophic matrix is a common strategy for invertebrates to cope with exogenous stressors that
224 have been consumed and enter the digestive tract.[61] The changes in expression of peritrophin
225 genes and other genes related to chitin synthesis and organization may indicate that alterations in
226 these environment-facing structures may be an important first-line response for invertebrates
227 encountering nanomaterials such as LCO in the environment.

228 Relatively few genes were identified as being differentially expressed (Wald FRD < 0.1)
229 between 1 mg/L LCO exposed larvae and controls, only 34 versus the 1409 differentially
230 expressed between 10 mg/L LCO and control. No molecular functions or pathways were
231 identified as statistically enriched by DAVID between 1mg/L LCO and control. However, of the
232 29 differentially expressed genes annotated by DAVID, eight, or more than a quarter, were
233 peptidases. This could indicate a shift toward protein catabolism even at an LCO exposure
234 concentration that did not cause observable effects on aconitase activity in this study (Fig 2) or
235 on growth or development in our previous study.[33] No differentially expressed genes were
236 detected between released ion exposure equivalent to ions released by 10 mg/L LCO and control,
237 demonstrating ENM-specific LCO impacts.

238

239 **Conclusions**

240 This work provides evidence for the oxidative disruption of Fe-S centers of proteins as a
241 molecular initiating event, and subsequent metabolic disruption as a key event, of the toxicity of
242 the complex transition metal oxide ENM LCO. A proposed AOP summarizing our findings and
243 how they relate to previous studies of LCO is included as Figure 5. We propose that ROS
244 generated by LCO[45] oxidizes the Fe-S center of aconitase (observed by EPR; Fig 1b) and likely
245 other Fe-S enzymes with solvent-exposed Fe-S centers. This results in lower enzyme activity
246 (observed for aconitase; Fig 2), which results in metabolic disruption and energy starvation
247 (observed by RNA-Seq; Figs 3 and 4) that lead to reduced growth and delayed adult
248 emergence.[33] The conservation of Fe-S proteins as important enzymatic and regulatory proteins
249 across species[42] suggests that this mechanism may also be broadly relevant, for LCO
250 specifically, and potentially for other transition metal oxide ENMs.

251

252 **Materials and methods**

253 ***LCO nanosheet synthesis and characterization***

254 Sheet-like Li_xCoO_2 nanoparticles were synthesized as described previously.[62] A cobalt hydroxide
255 ($Co(OH)_2$) precursor was synthesized by precipitation by adding a 0.1 M solution of LiOH in
256 420 mL 18.2 MΩ water (ultrapure water used here and in all future steps) dropwise to a 1 M
257 $Co(NO_3)_2 \cdot 6H_2O$ solution in 20 mL water ([OH] 5% stoichiometric excess for $Co^{2+} + 2OH^- \rightarrow$
258 $Co(OH)_2$). The resulting precipitate was immediately isolated by centrifugation at 4696 g for 3
259 min, redispersed in water to wash, and isolated by centrifugation again. Washing was repeated

260 two more times. The final supernatant was then decanted and the product dried in a 30 °C
261 vacuum oven overnight. The dried $Co(OH)_2$ product was then transformed to $LiCoO_2$ by adding
262 0.20 g of the $Co(OH)_2$ particles to a molten salt flux of 6:4 molar ratio of $LiNO_3$:LiOH (10 g
263 total) at 200 °C in a poly(tetrafluoroethylene) container with magnetic stirring assembled in a
264 silicone oil bath, forming Li_xCoO_2. After 30 min, the reaction was quenched with water, and
265 Li_xCoO_2 particles were isolated by centrifugation at 4969 g for 5 min. The particle pellet was
266 washed by redispersing in water and isolating by centrifugation three times. The final product
267 was dried in a vacuum oven overnight at 30 °C. To verify extent of lithiation, particles were
268 digested in aqua regia and analyzed via inductively coupled plasma – optical emission
269 spectroscopy, yielding a Li:Co ratio of 0.92:1. We refer to this composition, $Li_{0.92}CoO_2$ as
270 "LCO." Surface area measured by BET was determined to be 125 m^2/g. Particles were imaged
271 edge-on using scanning electron microscopy and showed sheet-like structures consistent with
272 previously published synthesis of this material (Supplementary Figure S5).[62] Size analysis from
273 the previously published synthesis showed approximate nanosheet diameters of 25 nm and
274 widths of 5 nm by transmission electron microscopy.[62] Powder X-Ray Diffraction patterns were
275 also consistent with previously published work that can be indexed to the $R\bar{3}m$ space group
276 (Supplementary Figure S6).[62] Zeta potential for these materials in exposure media was -12.6 ±
277 0.6 mV for 1 mg/L LCO and -3.7 ± 0.5 mV for 10 mg/L LCO, similar to previous results for
278 these materials in these conditions (Supplementary Table S1).[33]

279

280 ***RNA-Seq***

281 *Larval exposure*

282 *C. riparius* egg ropes were obtained from Aquatic Research Organisms (ARO; Hampton, NH).
283 Once hatched, larvae were fed once daily 0.5 mL of supernatant from finely ground TetraMin®
284 Tropical Flake fish food at 20 mg/mL for 2 d and the full Tetramin® suspension for another 3 d.
285 At 5 d post-hatch, animals were transferred to 100 mL exposure beakers containing 5 g 140-270
286 mesh fine silica sand (AGSCO Corp) and 20 mL 2x moderately hard reconstituted water
287 (MHRW).[43] Final exposures were made up by adding 20 mL of Milli-Q® ultrapure H_2O to
288 control beakers, Li and Co ions to a final concentration 660 µg/L Li as LiCl and 150 µg/L Co as
289 $CoCl_2$, equivalent to ions released by LCO at 10 mg/L in MHRW over 48 hr,[33] or LCO for final
290 concentrations of 1 and 10 mg/L. Five animals were added to each of 6 replicate beakers per
291 condition. Animals were fed 125 µL of 20 mg/mL finely ground Tetrmin® suspension per
292 beaker daily over the 48 hr exposure period. After 48 hr of exposure, animals were carefully
293 removed from exposure beakers, rinsed 3x in fresh 1x MHRW, flash frozen in liquid N_2, and
294 stored at -80 °C for subsequent RNA extraction, library creation, and sequencing.

295

296 *RNA-extraction, library prep, and sequencing*

297 Flash frozen larvae were homogenized in TRIzol and RNA purified using the Direct-zol RNA
298 MiniPrep (Zymo Research, R2051). RNA quality and yield were determined using the
299 NanoDrop 1000 spectrophotometer, Agilent Bioanalyzer 2100, and Qubit fluorometer. RNA
300 quality for all samples were as follows: 260/280 ratio 1.8-2.0, 260/230 ratio 2.0-2.2, and RIN >
301 7. 200ng of total RNA from each sample was used to prepare RNA sequencing libraries using
302 the Illumina TruSeq Stranded mRNA kit (Illumina, RS-122-2102) and IDT for Illumina –
303 TruSeq RNA UD Indexes (Illumina, 20022371). Libraries were sequenced on the Illumina
304 NovaSeq6000, with paired-end reads of 150 bp.

305

306 *Processing of RNA-Seq data*

307 Total genomic yield approached 996 million paired-end reads, median per-sample yield 49.45
308 million fragments, population standard deviation 16.77 million fragments, data was quality-
309 assessed using FastQC v0.11.5,[63] and no apparent base-calling errors were flagged for removal.
310 Cutadapt v1.18 was used to clip Illumina TruSeq 3'-anchored primers,[64] and Trinity v2.8.3 used
311 to *de novo* assemble the quality-controlled data into a draft reference transcriptome.[65]

312 In order to overcome poor annotation in available databases for *C. riparius*, the BLASTX aligner
313 within the NCBI-BLAST+ package v2.2.28 was used to iteratively annotate the assembly against
314 available NCBI proteins for *C. riparius*;[66] followed by the genome releases of well-annotated
315 fellow Nematocerans (Culicomorpha) *Anopheles gambiae*, *Culex quinquefasciatus*, and *Aedes*
316 *aegypti*;[67,68] and finally against the February 2019 release of UniProt-SwissProt. Kallisto v0.45.0
317 was then used to pseudoalign and sample-quantify paired-end data against the annotated draft
318 reference transcriptome.[69]

319 DESeq2 was used to perform differential expression analysis on sample pairs using R v3.5.3.[70]
320 Differentially expressed genes determined by DESeq2 were then re-annotated using reference
321 sequence metadata and joined relationally with Kallisto sample quantification counts using
322 custom tooling.

323

324 *Analysis of RNA-Seq data using DAVID and KEGG*

325 Differentially expressed, annotated contigs present in at least 80% of samples were analyzed for
326 function and functional enrichment using the Database for Annotation, Visualization and
327 Integrated Discovery (DAVID).[49,50] DAVID statistical enrichment was determined based on a
328 Banjamini-adjusted FDR < 0.1. The Kyoto Encyclopedia of Genes and Genomes (KEGG) was
329 used to assign KEGG orthology (KO) terms to annotated contigs and perform pathway
330 analysis.[71–73] A total of 28,101 contigs were successfully assembled and present in at least 80%
331 of samples. Of these 10,014 could be successfully annotated using BLASTX (e-value ≤ 0.1).
332 1409 annotated contigs were differentially expressed between control and 10 mg/L LCO samples
333 and found in at least 80% of samples (Wald FDR < 0.1). Of these 1,373 could be assigned
334 functions in DAVID and 354 could be assigned KOs by KEGG, of which 319 could be assigned
335 to pathways.

336

337 ***Aconitase enzyme activity assay***

338 Aconitase enzyme activity assays were carried out on protein extracted from exposed larvae
339 using the Cayman Chemical Aconitase Assay Kit (Cayman Chemical, 705502). Larvae were fed
340 and exposed as described above: control, released ion control, 1 mg/L LCO, 10 mg/L LCO for
341 48 hr. At 48 hr, larvae from 10 replicate beakers per condition (50 larvae total) were pooled and
342 homogenized in aconitase assay buffer on ice. Samples were centrifuged at 800 x g at 4 °C for 10
343 min and the supernatant of soluble protein harvested per kit instructions. Total protein
344 concentration was quantified using the Pierce™ BCA Protein Assay Kit (Thermo Scientific,
345 23225). Samples were assayed for activity using 500 µg/mL of total protein per aconitase kit
346 instructions. A total of 5 independent replicates per condition were assayed.

347

348 ***EPR measurements***

349 For EPR analysis, C. riparius larvae 5 dph were exposed to control, released ion control, and 10
350 mg/L LCO for 7 d. One egg rope (containing hundreds of larvae) was used for each of 5
351 replicates per condition. A high number of larvae per condition and increased exposure time
352 were used to ensure sufficient animal mass for the assay. Animals were loaded into Wilmad®
353 quartz (CFQ) O.D. 4 mm EPR tubes (Sigma-Aldrich, Z566535) cut to 14 cm and were first
354 frozen slowly and stored briefly in liquid N_2 to avoid the possibility of cracking inside the
355 cryostat of the EPR instrument. All samples were measured using a Bruker ELEXSYS E500 X-
356 Band CW- ESR spectrometer at a temperature of 10 K using a liquid helium ESR900 continuous
357 flow cryostat.

358 Spectra were analyzed using Mnova version 14.1.2 software with a beta version EPR plug-in
359 (Mestrelab). For quantitative analysis, all spectra were converted into their first integrals and
360 background-corrected to yield final spectra. The integrated area for peaks of interest were
361 obtained by double integration of the EPR spectra and were normalized by their ratio to the Mn^{2+}
362 peak at ~ 3250 G (g ~ 2.08) to account for differences in sample loading, an intrasample
363 normalization approach.[74,75] Specifically, the peaks of interest are: the peak at ~3350 G (g ~
364 2.02), characteristic of oxidized aconitase $[3Fe\text{-}4S]^{1+}$; the peak at ~ 3470 G (g ~ 1.98),
365 characteristic of Complex II $[3Fe\text{-}4S]^{1+}$; and the peak at ~ 3560 G (g ~ 1.91), characteristic of
366 Complex I and II $[2Fe\text{-}2S]^{1+}$ and $[4Fe\text{-}4S]^{1+}$.[38,74]

367

368 ***Statistics***

Data from EPR and aconitase assays were analyzed for normality using the Shapiro-Wilk test and equality of variance using Levene's test. Statistical significance of differences between treatments was determined using a One-way ANOVA with Tukey HSD post-hoc tests for data with equal variance and a One-way Welch ANOVA with Dunnett T3 post-hoc tests for data with unequal variance. Statistical tests were performed using SPSS version 23 for Mac.

Acknowledgement

This work was supported by National Science Foundation under the Center for Sustainable Nanotechnology (CSN), CHE-1503408. The CSN is part of the Centers for Chemical Innovation Program. This project used the UW-Milwaukee Great Lakes Genomics Center for RNA isolation, Illumina NovaSeq RNA sequencing, and bioinformatics services. EPR analysis was carried out at the UW-Madison Department of Chemistry's Paul Bender Chemical Instrumentation Center.

Conflict of interest statement

The authors have no conflicts to declare.

Supporting Information

Supporting information includes supplementary figures and tables referenced in the text and a list of relevant genes identified as differentially expressed by RNA-Seq. This material is available free of charge via the internet at http://pubs.acs.org.

390

391 **References**

392 (1) Klaper, R. D. The Known and Unknown about the Environmental Safety of
393 Nanomaterials in Commerce. *Small* **2020**, 2000690.
394 https://doi.org/10.1002/smll.202000690.

395 (2) Friedersdorf, L. E.; Bjorkland, R.; Klaper, R. D.; Sayes, C. M.; Wiesner, M. R. Fifteen
396 Years of NanoEHS Research Advances Science and Fosters a Vibrant Community. *Nat.*
397 *Nanotechnol.* **2019**, *14* (11), 996–998. https://doi.org/10.1038/s41565-019-0574-z.

398 (3) Maynard, A. D.; Warheit, D. B.; Philbert, M. A. The New Toxicology of Sophisticated
399 Materials: Nanotoxicology and Beyond. *Toxicol. Sci.* **2011**, *120* (Supplement 1), S109–
400 S129. https://doi.org/10.1093/toxsci/kfq372.

401 (4) Khanna, P.; Ong, C.; Bay, B.; Baeg, G.; Khanna, P.; Ong, C.; Bay, B. H.; Baeg, G. H.
402 Nanotoxicity: An Interplay of Oxidative Stress, Inflammation and Cell Death.
403 *Nanomaterials* **2015**, *5* (3), 1163–1180. https://doi.org/10.3390/nano5031163.

404 (5) Mendoza, R. P.; Brown, J. M. Engineered Nanomaterials and Oxidative Stress: Current
405 Understanding and Future Challenges. *Curr. Opin. Toxicol.* **2018**.
406 https://doi.org/10.1016/J.COTOX.2018.09.001.

407 (6) Manickam, V.; George, L.; Tanny, A.; Lochana, R.; Velusamy, R. K.; Kumar, M. M.;
408 Rajendran, B.; Tamizhselvi, R.; George, L.; Tanny, A.; et al. Methods and Protocols for In
409 Vitro Animal Nanotoxicity Evaluation: A Detailed Review. In *Nanotoxicology*; CRC
410 Press: Boca Raton : CRC Press, Taylor & Francis Group, 2018., 2018; pp 285–321.

411 https://doi.org/10.1201/b21545-12.

412 (7) Qiu, T. A.; Clement, P. L.; Haynes, C. L. Linking Nanomaterial Properties to Biological
413 Outcomes: Analytical Chemistry Challenges in Nanotoxicology for the next Decade.
414 *Chem. Commun.* **2018**, *54* (91), 12787–12803. https://doi.org/10.1039/C8CC06473C.

415 (8) Mittler, R. ROS Are Good. *Trends Plant Sci.* **2017**, *22* (1), 11–19.
416 https://doi.org/10.1016/J.TPLANTS.2016.08.002.

417 (9) Reczek, C. R.; Chandel, N. S. ROS-Dependent Signal Transduction. *Curr. Opin. Cell*
418 *Biol.* **2015**, *33*, 8–13. https://doi.org/10.1016/J.CEB.2014.09.010.

419 (10) Ray, P. D.; Huang, B.-W.; Tsuji, Y. Reactive Oxygen Species (ROS) Homeostasis and
420 Redox Regulation in Cellular Signaling. *Cell. Signal.* **2012**, *24* (5), 981–990.
421 https://doi.org/10.1016/J.CELLSIG.2012.01.008.

422 (11) Wang, K.; Jiang, J.; Lei, Y.; Zhou, S.; Wei, Y.; Huang, C. Targeting Metabolic–Redox
423 Circuits for Cancer Therapy. *Trends Biochem. Sci.* **2019**.
424 https://doi.org/10.1016/J.TIBS.2019.01.001.

425 (12) Diebold, L.; Chandel, N. S. Mitochondrial ROS Regulation of Proliferating Cells. *Free*
426 *Radic. Biol. Med.* **2016**, *100*, 86–93.
427 https://doi.org/10.1016/J.FREERADBIOMED.2016.04.198.

428 (13) Rampon, C.; Volovitch, M.; Joliot, A.; Vriz, S.; Rampon, C.; Volovitch, M.; Joliot, A.;
429 Vriz, S. Hydrogen Peroxide and Redox Regulation of Developments. *Antioxidants* **2018**, *7*
430 (11), 159. https://doi.org/10.3390/antiox7110159.

431 (14) Wen, X.; Wu, J.; Wang, F.; Liu, B.; Huang, C.; Wei, Y. Deconvoluting the Role of

Reactive Oxygen Species and Autophagy in Human Diseases. *Free Radic. Biol. Med.* **2013**, *65*, 402–410. https://doi.org/10.1016/J.FREERADBIOMED.2013.07.013.

(15) Redza-Dutordoir, M.; Averill-Bates, D. A. Activation of Apoptosis Signalling Pathways by Reactive Oxygen Species. *Biochim. Biophys. Acta - Mol. Cell Res.* **2016**, *1863* (12), 2977–2992. https://doi.org/10.1016/J.BBAMCR.2016.09.012.

(16) Boyes, W. K.; Thornton, B. L. M.; Al-Abed, S. R.; Andersen, C. P.; Bouchard, D. C.; Burgess, R. M.; Hubal, E. A. C.; Ho, K. T.; Hughes, M. F.; Kitchin, K.; et al. A Comprehensive Framework for Evaluating the Environmental Health and Safety Implications of Engineered Nanomaterials. *Crit. Rev. Toxicol.* **2017**, *47* (9), 771–814. https://doi.org/10.1080/10408444.2017.1328400.

(17) Gerloff, K.; Landesmann, B.; Worth, A.; Munn, S.; Palosaari, T.; Whelan, M. The Adverse Outcome Pathway Approach in Nanotoxicology. *Comput. Toxicol.* **2017**, *1*, 3–11. https://doi.org/10.1016/J.COMTOX.2016.07.001.

(18) Halappanavar, S.; Ede, J. D.; Shatkin, J. A.; Krug, H. F. A Systematic Process for Identifying Key Events for Advancing the Development of Nanomaterial Relevant Adverse Outcome Pathways. *NanoImpact* **2019**, *15*, 100178. https://doi.org/10.1016/J.IMPACT.2019.100178.

(19) Allen, T. E. H.; Goodman, J. M.; Gutsell, S.; Russell, P. J. Defining Molecular Initiating Events in the Adverse Outcome Pathway Framework for Risk Assessment. *Chem. Res. Toxicol.* **2014**, *27* (12), 2100–2112. https://doi.org/10.1021/tx500345j.

(20) Brodd, R. J. *Batteries for Sustainability : Selected Entries from the Encyclopedia of Sustainability Science and Technology*; Springer, 2012.

454 (21) Grey, C. P.; Ceder, G.; Kang, K.; Meng, Y. S.; Bre, J. Electrodes with High Power and
455 High Capacity for Rechargeable Lithium Batteries. *Science (80-.).* **2005**, *311* (December),
456 1–5. https://doi.org/10.1126/science.1122152.

457 (22) Pollet, B. G.; Staffell, I.; Shang, J. L. Current Status of Hybrid, Battery and Fuel Cell
458 Electric Vehicles: From Electrochemistry to Market Prospects. *Electrochim. Acta* **2012**,
459 *84*, 235–249. https://doi.org/10.1016/j.electacta.2012.03.172.

460 (23) Wang, Y.; Yu, Y.; Huang, K.; Chen, B.; Deng, W.; Yao, Y. Quantifying the
461 Environmental Impact of a Li-Rich High-Capacity Cathode Material in Electric Vehicles
462 via Life Cycle Assessment. *Environ. Sci. Pollut. Res.* **2017**, *24* (2), 1251–1260.
463 https://doi.org/10.1007/s11356-016-7849-9.

464 (24) Winslow, K. M.; Laux, S. J.; Townsend, T. G. A Review on the Growing Concern and
465 Potential Management Strategies of Waste Lithium-Ion Batteries. *Resources,*
466 *Conservation and Recycling*. Elsevier 2018, pp 263–277.
467 https://doi.org/10.1016/j.resconrec.2017.11.001.

468 (25) Hamers, R. J. Nanomaterials and Global Sustainability. *Acc. Chem. Res.* **2017**, *50* (3),
469 633–637. https://doi.org/10.1021/acs.accounts.6b00634.

470 (26) Armitage, P. D.; Cranston, P. S.; Pinder, L. C. V. *The Chironomidae : Biology and*
471 *Ecology of Non-Biting Midges*, 1st ed.; Chapman & Hall, 1995.

472 (27) Besten, P. J. den.; Munawar, M. *Ecotoxicological Testing of Marine and Freshwater*
473 *Ecosystems : Emerging Techniques, Trends, and Strategies*; Taylor & Francis, 2005.

474 (28) Park, S.-Y.; Chung, J.; Colman, B. P.; Matson, C. W.; Kim, Y.; Lee, B.-C.; Kim, P.-J.;

Choi, K.; Choi, J. Ecotoxicity of Bare and Coated Silver Nanoparticles in the Aquatic Midge, Chironomus Riparius. *Environ. Toxicol. Chem.* **2015**, *34* (9), 2023–2032. https://doi.org/10.1002/etc.3019.

(29) Gopalakrishnan Nair, P. M.; Chung, I. M. Alteration in the Expression of Antioxidant and Detoxification Genes in Chironomus Riparius Exposed to Zinc Oxide Nanoparticles. *Comp. Biochem. Physiol. Part B Biochem. Mol. Biol.* **2015**, *190*, 1–7. https://doi.org/10.1016/j.cbpb.2015.08.004.

(30) Waissi-Leinonen, G. C.; Petersen, E. J.; Pakarinen, K.; Akkanen, J.; Leppänen, M. T.; Kukkonen, J. V. K. Toxicity of Fullerene (C60) to Sediment-Dwelling Invertebrate Chironomus Riparius Larvae. *Environ. Toxicol. Chem.* **2012**, *31* (9), 2108–2116. https://doi.org/10.1002/etc.1926.

(31) Nair, P. M. G.; Park, S. Y.; Lee, S.-W.; Choi, J. Differential Expression of Ribosomal Protein Gene, Gonadotrophin Releasing Hormone Gene and Balbiani Ring Protein Gene in Silver Nanoparticles Exposed Chironomus Riparius. *Aquat. Toxicol.* **2011**, *101* (1), 31–37. https://doi.org/10.1016/j.aquatox.2010.08.013.

(32) Lee, S.-W.; Kim, S.-M.; Choi, J. Genotoxicity and Ecotoxicity Assays Using the Freshwater Crustacean Daphnia Magna and the Larva of the Aquatic Midge Chironomus Riparius to Screen the Ecological Risks of Nanoparticle Exposure. *Environ. Toxicol. Pharmacol.* **2009**, *28* (1), 86–91. https://doi.org/10.1016/j.etap.2009.03.001.

(33) Niemuth, N. J.; Curtis, B. J.; Hang, M. N.; Gallagher, M. J.; Fairbrother, D. H.; Hamers, R. J.; Klaper, R. D. Next-Generation Complex Metal Oxide Nanomaterials Negatively Impact Growth and Development in the Benthic Invertebrate Chironomus Riparius upon

497 Settling. *Environ. Sci. Technol.* **2019**, *53* (7), 3860–3870.
498 https://doi.org/10.1021/acs.est.8b06804.

499 (34) Beinert, H. Iron-Sulfur Proteins: Ancient Structures, Still Full of Surprises. *Journal of*
500 *Biological Inorganic Chemistry*. Springer-Verlag February 2000, pp 2–15.
501 https://doi.org/10.1007/s007750050002.

502 (35) Castello, A.; Hentze, M. W.; Preiss, T. Metabolic Enzymes Enjoying New Partnerships as
503 RNA-Binding Proteins. *Trends Endocrinol. Metab.* **2015**, *26* (12), 746–757.
504 https://doi.org/10.1016/j.tem.2015.09.012.

505 (36) Resch, V.; Hanefeld, U. The Selective Addition of Water. *Catal. Sci. Technol.* **2015**, *5* (3),
506 1385–1399. https://doi.org/10.1039/C4CY00692E.

507 (37) Tong, J.; Feinberg, B. A. Direct Square-Wave Voltammetry of Superoxidized [4Fe-4S]3+
508 Aconitase and Associated 3Fe/4Fe Cluster Interconversions. *J. Biol. Chem.* **1994**, *269*
509 (40), 24920–24927.

510 (38) Kalyanaraman, B.; Cheng, G.; Zielonka, J.; Bennett, B. Low-Temperature EPR
511 Spectroscopy as a Probe-Free Technique for Monitoring Oxidants Formed in Tumor Cells
512 and Tissues: Implications in Drug Resistance and OXPHOS-Targeted Therapies. *Cell*
513 *Biochem. Biophys.* **2019**, *77* (1), 89–98. https://doi.org/10.1007/s12013-018-0858-1.

514 (39) Sazanov, L. A. A Giant Molecular Proton Pump: Structure and Mechanism of Respiratory
515 Complex I. *Nat. Rev. Mol. Cell Biol.* **2015**, *16* (6), 375–388.
516 https://doi.org/10.1038/nrm3997.

517 (40) Van Vranken, J. G.; Na, U.; Winge, D. R.; Rutter, J. Protein-Mediated Assembly of

518 Succinate Dehydrogenase and Its Cofactors. *Crit. Rev. Biochem. Mol. Biol.* **2015**, *50* (2),
519 168–180. https://doi.org/10.3109/10409238.2014.990556.

520 (41) Barras, F.; Fontecave, M. Cobalt Stress in Escherichia Coli and Salmonella Enterica:
521 Molecular Bases for Toxicity and Resistance. *Metallomics* **2011**, *3* (11), 1130–1134.
522 https://doi.org/10.1039/c1mt00099c.

523 (42) Lill, R.; Mühlenhoff, U. Iron–Sulfur-Protein Biogenesis in Eukaryotes. *Trends Biochem.*
524 *Sci.* **2005**, *30* (3), 133–141. https://doi.org/10.1016/j.tibs.2005.01.006.

525 (43) Bozich, J.; Hang, M.; Hamers, R.; Klaper, R. Core Chemistry Influences the Toxicity of
526 Multicomponent Metal Oxide Nanomaterials, Lithium Nickel Manganese Cobalt Oxide,
527 and Lithium Cobalt Oxide to Daphnia Magna. *Environ. Toxicol. Chem.* **2017**, *36* (9),
528 2493–2502. https://doi.org/10.1002/etc.3791.

529 (44) Sironval, V.; Reylandt, L.; Chaurand, P.; Ibouraadaten, S.; Palmai-Pallag, M.; Yakoub,
530 Y.; Ucakar, B.; Rose, J.; Poleunis, C.; Vanbever, R.; et al. Respiratory Hazard of Li-Ion
531 Battery Components: Elective Toxicity of Lithium Cobalt Oxide (LiCoO2) Particles in a
532 Mouse Bioassay. *Arch. Toxicol.* **2018**, *92* (5), 1673–1684. https://doi.org/10.1007/s00204-
533 018-2188-x.

534 (45) Melby, E. S.; Cui, Y.; Borgatta, J.; Mensch, A. C.; Hang, M. N.; Chrisler, W. B.;
535 Dohnalkova, A.; Van Gilder, J. M.; Alvarez, C. M.; Smith, J. N.; et al. Impact of Lithiated
536 Cobalt Oxide and Phosphate Nanoparticles on Rainbow Trout Gill Epithelial Cells.
537 *Nanotoxicology* **2018**, *12* (10), 1166–1181.
538 https://doi.org/10.1080/17435390.2018.1508785.

539 (46) Hamers, R. J. Energy Storage Materials as Emerging Nano-Contaminants. *Chem. Res.*

540 *Toxicol.* **2020**, acs.chemrestox.0c00080. https://doi.org/10.1021/acs.chemrestox.0c00080.

541 (47) Ranquet, C.; Ollagnier-de-Choudens, S.; Loiseau, L.; Barras, F.; Fontecave, M. Cobalt
542 Stress in Escherichia Coli. The Effect on the Iron-Sulfur Proteins. *J. Biol. Chem.* **2007**,
543 *282* (42), 30442–30451. https://doi.org/10.1074/jbc.M702519200.

544 (48) Pearce, L. L.; Martinez-Bosch, S.; Manzano, E. L.; Winnica, D. E.; Epperly, M. W.;
545 Peterson, J. The Resistance of Electron-Transport Chain Fe–S Clusters to Oxidative
546 Damage during the Reaction of Peroxynitrite with Mitochondrial Complex II and Rat-
547 Heart Pericardium. *Nitric Oxide* **2009**, *20* (3), 135–142.
548 https://doi.org/10.1016/j.niox.2008.12.001.

549 (49) Huang, D. W.; Sherman, B. T.; Lempicki, R. A. Systematic and Integrative Analysis of
550 Large Gene Lists Using DAVID Bioinformatics Resources. *Nat. Protoc.* **2009**, *4* (1), 44–
551 57. https://doi.org/10.1038/nprot.2008.211.

552 (50) Huang, D. W.; Sherman, B. T.; Lempicki, R. A. Bioinformatics Enrichment Tools: Paths
553 toward the Comprehensive Functional Analysis of Large Gene Lists. *Nucleic Acids Res.*
554 **2009**, *37* (1), 1–13. https://doi.org/10.1093/nar/gkn923.

555 (51) Rouault, T. A.; Tong, W. H. Iron–Sulfur Cluster Biogenesis and Human Disease. *Trends*
556 *Genet.* **2008**, *24* (8), 398–407. https://doi.org/10.1016/j.tig.2008.05.008.

557 (52) Filippi, C.; Pryde, A.; Cowan, P.; Lee, T.; Hayes, P.; Donaldson, K.; Plevris, J.; Stone, V.
558 Toxicology of ZnO and TiO 2 Nanoparticles on Hepatocytes: Impact on Metabolism and
559 Bioenergetics. *Nanotoxicology* **2015**, *9* (1), 126–134.
560 https://doi.org/10.3109/17435390.2014.895437.

561 (53) Yan, G.; Huang, Y.; Bu, Q.; Lv, L.; Deng, P.; Zhou, J.; Wang, Y.; Yang, Y.; Liu, Q.; Cen,
562 X.; et al. Zinc Oxide Nanoparticles Cause Nephrotoxicity and Kidney Metabolism
563 Alterations in Rats. *J. Environ. Sci. Heal. Part A* **2012**, *47* (4), 577–588.
564 https://doi.org/10.1080/10934529.2012.650576.

565 (54) Chai, H.; Yao, J.; Sun, J.; Zhang, C.; Liu, W.; Zhu, M.; Ceccanti, B. The Effect of Metal
566 Oxide Nanoparticles on Functional Bacteria and Metabolic Profiles in Agricultural Soil.
567 *Bull. Environ. Contam. Toxicol.* **2015**, *94* (4), 490–495. https://doi.org/10.1007/s00128-
568 015-1485-9.

569 (55) Cardinale, B. J.; Bier, R.; Kwan, C. Effects of TiO2 Nanoparticles on the Growth and
570 Metabolism of Three Species of Freshwater Algae. *J. Nanoparticle Res.* **2012**, *14* (8), 913.
571 https://doi.org/10.1007/s11051-012-0913-6.

572 (56) Ratnasekhar, C.; Sonane, M.; Satish, A.; Mudiam, M. K. R. Metabolomics Reveals the
573 Perturbations in the Metabolome of Caenorhabditis Elegans Exposed to Titanium Dioxide
574 Nanoparticles. *Nanotoxicology* **2015**, *9* (8), 994–1004.
575 https://doi.org/10.3109/17435390.2014.993345.

576 (57) Dieni, C. A.; Callaghan, N. I.; Gormley, P. T.; Butler, K. M. A.; MacCormack, T. J.
577 Physiological Hepatic Response to Zinc Oxide Nanoparticle Exposure in the White
578 Sucker, Catostomus Commersonii. *Comp. Biochem. Physiol. Part C Toxicol. Pharmacol.*
579 **2014**, *162*, 51–61. https://doi.org/10.1016/j.cbpc.2014.03.009.

580 (58) Guo, J.; Gao, S.-H.; Lu, J.; Bond, P. L.; Verstraete, W.; Yuan, Z. Copper Oxide
581 Nanoparticles Induce Lysogenic Bacteriophage and Metal-Resistance Genes in
582 Pseudomonas Aeruginosa PAO1. *ACS Appl. Mater. Interfaces* **2017**, *9* (27), 22298–

583 22307. https://doi.org/10.1021/acsami.7b06433.

584 (59) Tedesco, S.; Bayat, N.; Danielsson, G.; Buque, X.; Aspichueta, P.; Fresnedo, O.;
585 Cristobal, S. Proteomic and Lipidomic Analysis of Primary Mouse Hepatocytes Exposed
586 to Metal and Metal Oxide Nanoparticles. *J. Integr. OMICS* **2015**, *5* (1).
587 https://doi.org/10.5584/jiomics.v5i1.184.

588 (60) Merzendorfer, H. Chitin Metabolism in Insects: Structure, Function and Regulation of
589 Chitin Synthases and Chitinases. *J. Exp. Biol.* **2003**, *206* (24), 4393–4412.
590 https://doi.org/10.1242/jeb.00709.

591 (61) Lehane, M. J. PERITROPHIC MATRIX STRUCTURE AND FUNCTION. *Annu. Rev.*
592 *Entomol.* **1997**, *42* (1), 525–550. https://doi.org/10.1146/annurev.ento.42.1.525.

593 (62) Laudadio, E. D.; Bennett, J. W.; Green, C. M.; Mason, S. E.; Hamers, R. J. Impact of
594 Phosphate Adsorption on Complex Cobalt Oxide Nanoparticle Dispersibility in Aqueous
595 Media. *Environ. Sci. Technol.* **2018**, *52* (17), 10186–10195.
596 https://doi.org/10.1021/acs.est.8b02324.

597 (63) Andrews, S.; Krueger, F.; Seconds-Pichon, A.; Biggins, F.; Wingett, S. FastQC: A Quality
598 Control Tool for High Throughput Sequence Data. Babraham Bioinformatics, Babraham
599 Institute, Cambridge, United Kingdom 2010.

600 (64) Martin, M. Cutadapt Removes Adapter Sequences from High-Throughput Sequencing
601 Reads. *EMBnet.journal* **2011**, *17* (1), 10. https://doi.org/10.14806/ej.17.1.200.

602 (65) Grabherr, M. G.; Haas, B. J.; Yassour, M.; Levin, J. Z.; Thompson, D. A.; Amit, I.;
603 Adiconis, X.; Fan, L.; Raychowdhury, R.; Zeng, Q.; et al. Full-Length Transcriptome

604 Assembly from RNA-Seq Data without a Reference Genome. *Nat. Biotechnol.* **2011**, *29*
605 (7), 644–652. https://doi.org/10.1038/nbt.1883.

606 (66) Camacho, C.; Coulouris, G.; Avagyan, V.; Ma, N.; Papadopoulos, J.; Bealer, K.; Madden,
607 T. L. BLAST+: Architecture and Applications. *BMC Bioinformatics* **2009**, *10* (1), 421.
608 https://doi.org/10.1186/1471-2105-10-421.

609 (67) Marinković, M.; de Leeuw, W. C.; de Jong, M.; Kraak, M. H. S.; Admiraal, W.; Breit, T.
610 M.; Jonker, M. J. Combining Next-Generation Sequencing and Microarray Technology
611 into a Transcriptomics Approach for the Non-Model Organism Chironomus Riparius.
612 *PLoS One* **2012**, *7* (10), e48096. https://doi.org/10.1371/journal.pone.0048096.

613 (68) Nair, P. M. G.; Park, S. Y.; Choi, J. Analyses of Expressed Sequence Tags from
614 Chironomus Riparius Using Pyrosequencing : Molecular Ecotoxicology Perspective.
615 *Environ. Health Toxicol.* **2011**, *26*, e2011010.
616 https://doi.org/10.5620/eht.2011.26.e2011010.

617 (69) Bray, N. L.; Pimentel, H.; Melsted, P.; Pachter, L. Near-Optimal Probabilistic RNA-Seq
618 Quantification. *Nat. Biotechnol.* **2016**, *34* (5), 525–527. https://doi.org/10.1038/nbt.3519.

619 (70) Love, M. I.; Huber, W.; Anders, S. Moderated Estimation of Fold Change and Dispersion
620 for RNA-Seq Data with DESeq2. *Genome Biol.* **2014**, *15* (12), 550.
621 https://doi.org/10.1186/s13059-014-0550-8.

622 (71) Kanehisa, M.; Goto, S. KEGG: Kyoto Encyclopedia of Genes and Genomes. *Nucleic*
623 *Acids Res.* **2000**, *28* (1), 27–30. https://doi.org/10.1093/nar/28.1.27.

624 (72) Kanehisa, M.; Sato, Y.; Furumichi, M.; Morishima, K.; Tanabe, M. New Approach for

625 Understanding Genome Variations in KEGG. *Nucleic Acids Res.* **2019**, *47* (D1), D590–
626 D595. https://doi.org/10.1093/nar/gky962.

627 (73) Kanehisa, M. Toward Understanding the Origin and Evolution of Cellular Organisms.
628 *Protein Sci.* **2019**, *28* (11), 1947–1951. https://doi.org/10.1002/pro.3715.

629 (74) Haddy, A.; Smith, G. Transition Metal and Organic Radical Components of Carp Liver
630 Tissue Observed by Electron Paramagnetic Resonance Spectroscopy. *Comp. Biochem.*
631 *Physiol. Part B Biochem. Mol. Biol.* **1999**, *123* (4), 407–415.
632 https://doi.org/10.1016/S0305-0491(99)00087-5.

633 (75) Borzone, G.; Zhao, B.; Merola, A. J.; Berliner, L.; Clanton, T. L. Detection of Free
634 Radicals by Electron Spin Resonance in Rat Diaphragm after Resistive Loading. *J. Appl.*
635 *Physiol.* **1994**, *77* (2), 812–818. https://doi.org/10.1152/jappl.1994.77.2.812.

636

637

638 **Figures**

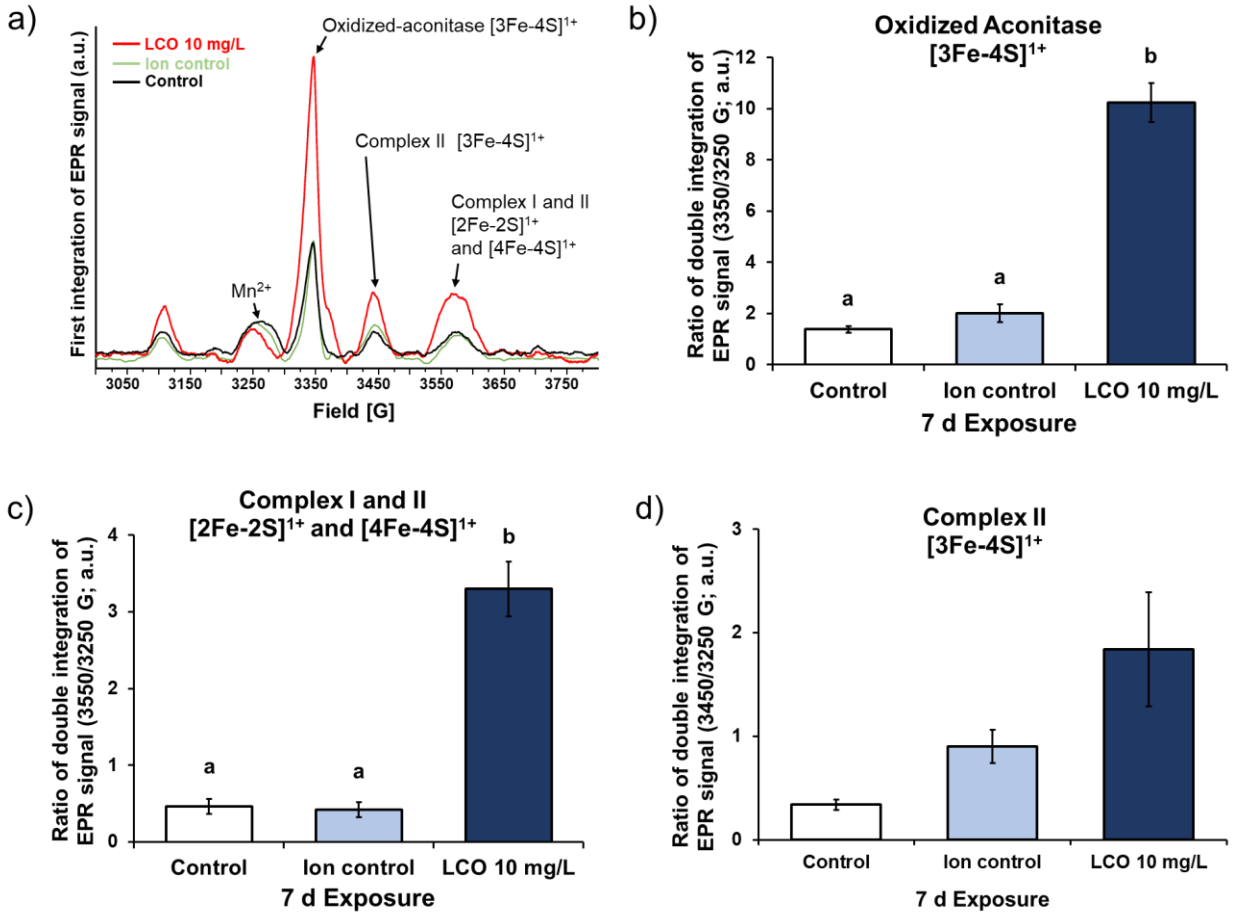

639 **Figure 1. Electron paramagnetic resonance spectroscopy of intact larvae shows changes in**

640 **Fe-S centers from LCO exposure**.

641

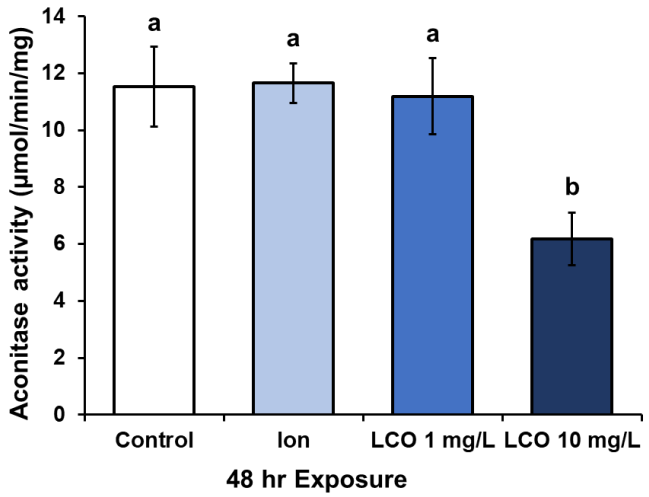

Figure 2. Aconitase activity of larval protein is negatively impacted by LCO.

644

Table 1. Differentially expressed Fe-S protein genes by function.

Function	Gene name	Pathway	Fold Direction
4Fe-4S binding			
	NUBP2; nucleotide binding protein 2	Iron-sulfur cluster assembly	UP
	NUBP1; nucleotide binding protein 1	Iron-sulfur cluster assembly	UP
	ISCA2; iron-sulfur cluster assembly 2	Iron-sulfur cluster assembly	UP
	SDHB; succinate dehydrogenase (ubiquinone) iron-sulfur subunit	Citrate cycle (TCA cycle), Oxidative phosphorylation	UP
	NDUFS7; NADH dehydrogenase (ubiquinone) Fe-S protein 7	Oxidative phosphorylation	UP
	NDUFV1; NADH dehydrogenase (ubiquinone) flavoprotein 1	Oxidative phosphorylation	UP
	NDUFS8; NADH dehydrogenase (ubiquinone) Fe-S protein 8	Oxidative phosphorylation	UP
	LIPA; lipoyl synthase	Lipoic acid metabolism	UP
	NTH; endonuclease III	Base excision repair	UP
	RTEL1; regulator of telomere elongation helicase 1	Telomere maintenance, DNA replication, DNA repair	UP
Fe-S biogenesis			
	ISCS; cysteine desulfurase	[2Fe-2S] cluster assembly	UP
Fe-S binding			
	Amidophosphoribosyl transferase	Purine metabolism	DOWN
	XDH; xanthine dehydrogenase/oxidase	Purine metabolism	UP

645

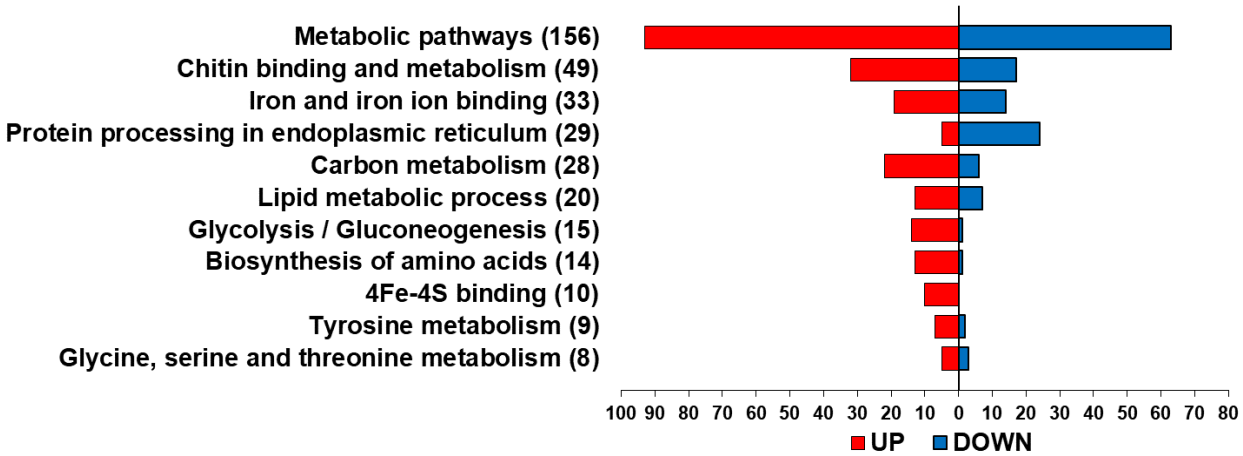

646 **Figure 3. Significantly enriched molecular functions and pathways show importance of**

647 **metabolism and Fe-S centers in LCO impacts.**

648

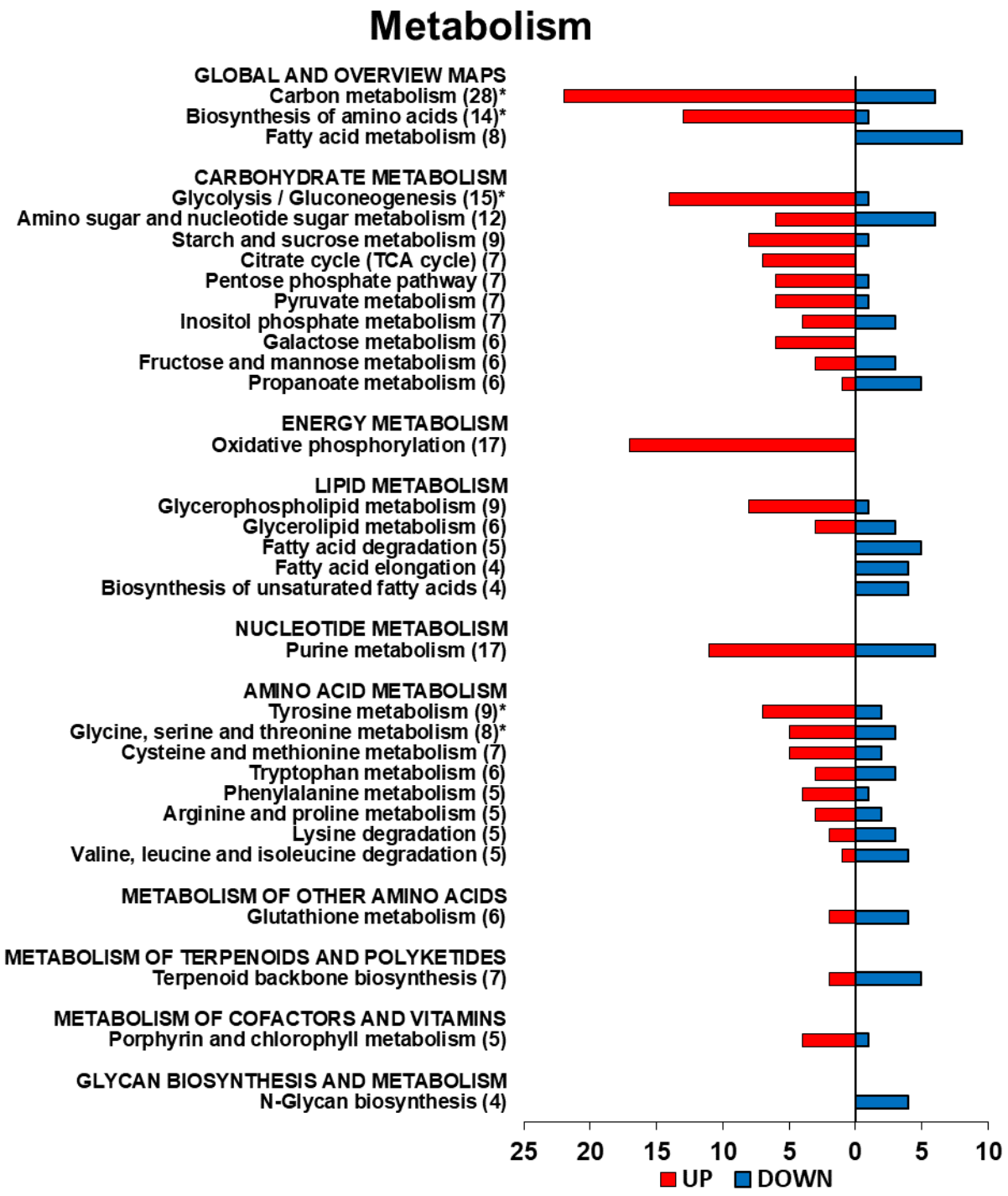

649 **Figure 4. Differentially expressed metabolic gene pathways indicate shift toward energy**

650 **production in LCO-exposed larvae.**

651

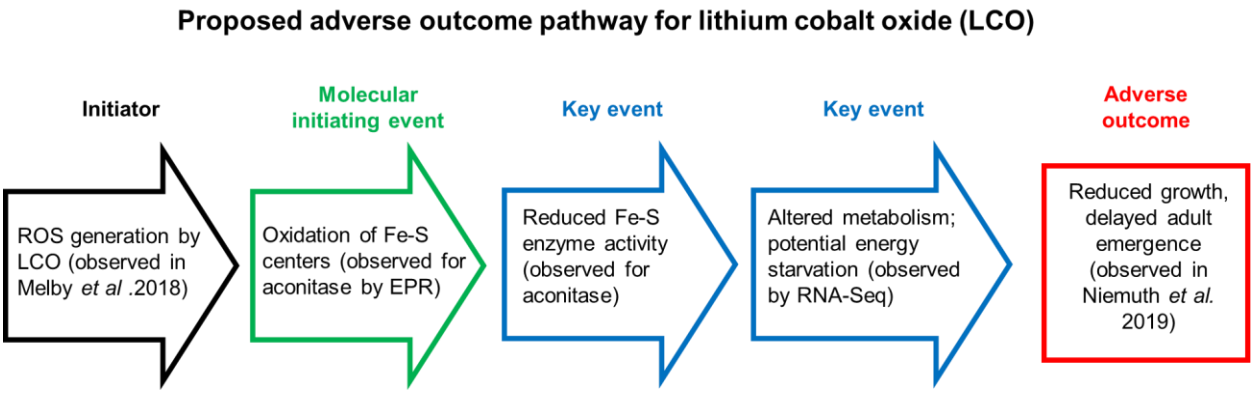

652 **Figure 5. Proposed adverse outcome pathway showing observed LCO impacts from**
653 **molecular initiating event through adverse outcomes.**

654

655 **Figure Legends**

656 **Figure 1. Electron paramagnetic resonance spectroscopy of intact larvae shows changes in**
657 **Fe-S centers from LCO exposure**. Representative electron paramagnetic resonance spectra (a)
658 for *C. riparius* larvae exposed to control, released Li and Co ion control, and 10 mg/L LCO for 7
659 days; and quantification of peak area for (b) oxidized aconitase $[3Fe\text{-}4S]^{1+}$, (c) [2Fe-2S]+ and
660 [4Fe-4S]+ from complex I and II of the electron transport chain (ETC), and (d) $[3Fe\text{-}4S]^{1+}$ from
661 complex I of the ETC relative to the peak area for Mn2+, which was invariant across samples.
662 Letters (panels b-d) indicate significant differences by one-way Welch ANOVA with Dunnett T3
663 post-hoc, $p < 0.05$. Average of 5 replicate samples; error bars indicate standard error of the mean.
664 Increased oxidation of the aconitase Fe-S center in LCO-exposed larvae identifies these sites as a
665 target of LCO-induced oxidative stress.

666 **Figure 2. Aconitase activity of larval protein is negatively impacted by LCO.** Aconitase
667 activity of protein extracted from *C. riparius* larvae exposed to control, released Li and Co ion
668 control, 1 mg/L LCO, and 10 mg/L LCO for 48 hr. Letters indicate significant differences by

669 One-way ANOVA with Tukey HSD post-hoc, $p < 0.05$. Average of 5 replicate samples; error
670 bars indicate standard error of the mean. The significant reduction in aconitase activity in 10
671 mg/L LCO-exposed larvae supports disruption of the Fe-S center of this enzyme as a potential
672 mechanism of LCO impact.

673 **Figure 3. Significantly enriched molecular functions and pathways show importance of**
674 **metabolism and Fe-S centers in LCO impacts.** Molecular functions and pathways identified as
675 significantly enriched (Benjamini-adjusted FDR < 0.1) in genes differentially expressed (Wald
676 FDR < 0.1) between control and 10 mg/L LCO-exposed *C. riarius* larvae at 48 hr by the
677 Database for Annotation, Visualization and Integrated Discovery (DAVID) v6.8. Metabolic
678 pathways are significantly enriched (156 genes), which includes Carbon metabolism (28 genes),
679 Lipid metabolic processes (20 genes), Glycolysis/Gluconeogenesis (15 genes), Biosynthesis of
680 amino acids (14 genes), Tyrosine metabolism (9 genes), and Glycine, serine and threonine
681 metabolism (8 genes) all being significantly enriched. Molecular functions significantly enriched
682 include Chitin binding and metabolism (49 genes), Iron and iron ion binding (33 genes), and
683 4Fe-4S binding (10 genes). Changes in Fe-S centers could potentially induce observed
684 differences in metabolism and iron ion binding because of their role in enzymatic and regulatory
685 proteins involved in these processes.

686 **Figure 4. Differentially expressed metabolic gene pathways indicate shift toward energy**
687 **production in LCO-exposed larvae.** Breakdown of Kyoto Encyclopedia of Genes and
688 Genomes (KEGG) pathways containing genes identified as differentially expressed (Wald FDR
689 < 0.1) between control and 10 mg/L LCO-exposed *C. riparius* larvae at 48 hr. * Indicates
690 specific pathways identified as significantly enriched by DAVID (Benjamini-adjusted FDR <
691 0.1; Fig 3). Overall metabolic changes, specifically changes in Carbon metabolism (28 genes),

692 including Glycolysis/gluconeogenesis (15 genes), the Citrate cycle (7 genes), and Oxidative
693 phosphorylation (17 genes), indicate a shift toward energy production in exposed larvae. The
694 critical role of Fe-S proteins in the Citrate cycle and Oxidative phosphorylation and their
695 disruption by LCO exposure could potentially explain observed changes.

696 **Figure 5. Proposed adverse outcome pathway showing observed LCO impacts from**
697 **molecular initiating event through adverse outcomes.** In the proposed adverse outcome
698 pathway (AOP), reactive oxygen species (ROS) generated by LCO (observed in Melby *et al*.
699 2018)[45] oxidize the of Fe-S centers in regulatory and metabolic proteins (observed for aconitase
700 in this study by electron paramagnetic resonance), reducing Fe-S enzyme activity (observed for
701 aconitase in this study) and changing regulatory activity. This disrupts metabolism, particularly
702 energy generation (observed in this study by RNA-Seq), ultimately causing reductions in growth
703 of larvae and delaying their development into adult flies (observe in Niemuth *et al*. 2019).[33]